Materials Research. 2017; 20(Suppl. 2): 181-189
DOI: http://dx.doi.org/10.1590/1980-5373-MR-2016-0936

Evaluation of the Photocatalytic Potential of TiO_2 and ZnO Obtained by Different Wet Chemical Methods

Patrícia Gonçalves[a]*, Roberto Bertholdo[a], Jeferson Almeida Dias[b], Sylma Carvalho Maestrelli[a], Tania Regina Giraldi[a]

[a]*Universidade Federal de Alfenas, campus Poços de Caldas, Rod. José Aurélio Vilela, BR 267, Km 533, 11999, Zip Code 37715-400, Poços de Caldas, MG, Brazil*
[b]*Universidade Federal de São Carlos, Rod. Washington Luiz, Km 235, Zip Code 13565-905, São Carlos, SP, Brazil*

Received: December 07, 2016; Revised: May 18, 2017; Accepted: May 22, 2017

This paper describes the development of TiO_2 and ZnO particles by a chemical route, using two different wet synthesis methods: polymeric precursor (PP) and sol-gel (SG). This study aimed to shed a light on how the synthesis method affects the photocatalytic activity of these oxides. Rhodamine B (RhB) degradation was used as a probe reaction to test the as-synthesized TiO_2 and ZnO photoactivity. It was observed that surface availability, which is related to the presence of synthesis residue, is the key parameter to determine photoactivity. ZnO PP and ZnO SG presented degradation of 88% to RhB. Both samples presented synthesis residue on the surface. On the other hand, TiO_2 PP presented a better performance than TiO_2 SG, once 90% of RhB was degraded, while TiO_2 SG degraded 80% of the dye. In this case, TiO_2 PP was free of synthesis residue on the surface, while TiO_2 SG presented residues.

Keywords: *TiO_2, ZnO, Rhodamine B, photocatalysis*

1. Introduction

Water contamination generated by dyes originating from the textile industries is a growing problem[1–4] since these pollutants typically show color and toxicity even in low concentration[5-6]. Several processes have been used to promote the water decontamination, among them physical and chemical processes. Physical processes including adsorption, coagulation, and flocculation[7-9]. These processes allow the removal of pollutants from the environment but do not promote their degradation. On the other hand, chemical processes can be used to promote water treatment by the oxidation of organic molecules (pollutants). Among those, a particular case is the photocatalysis, where a semiconductor surface is activated by UV-light to generate free radicals from OH• adsorbed species. These radicals are responsible for the degradation of contaminants such as organic molecules[10]. The more efficient semiconductors that promote photocatalysis are TiO_2 and ZnO[11-14]. These semiconductors present band gap suitable for such process, which allows for degrading of 100% of dyes in a short time[15,16]. However, several factors can interfere with the catalytic activity of these materials[17,18], e.g., the method of synthesis[19], the presence of surface contaminants[20-22], particle shapes[23], etc.

Han et al.[24] synthesized TiO_2 at low temperatures, by varying the pH and the ions present in the synthesis environment. The photocatalytic tests with these samples showed the influence of the morphology on the photocatalytic efficiency of the material, being this result justified in terms of the specific surface area of each morphology. Xie et al.[25] studied morphological control reports on TiO_2 nanocrystals synthesized via the solvothermal method, with the introduction of ethylenediamine (EDA). In this synthesis, EDA acts as a growth inhibitor, since without EDA nanowires were obtained, and after its introduction into the synthesis, nanofibers were also obtained. McLaren et al.[23] investigated the photocatalytic activity in the decomposition of methylene blue in aqueous solution as a function of average ZnO morphology. The authors verified a correlation of the properties of the shape factor, despite not having observed any apparent dependence on particle size. Similar results were reported by Yu et al.[26] in studies on the decolorization of RhB aqueous solutions photocatalyzed by ZnO hollow spheres with porous crystalline shells. Zheng et al.[27] synthesized hydrothermally uniform single-crystalline ZnO nanodisks and nanowires with well-defined crystal planes. It was demonstrated that the ZnO nanodisks with a high population of (0001) facet show higher catalytic activity by the comparison of photodegradation of RhB with ZnO nanowires used as the catalyst. The authors suggest that catalysts may be designed and synthesized to optimize the catalytic activity of nanocrystalline with well-defined active facets.

Despite the comprehensive literature about TiO_2 and ZnO properties, as well as several studies about the effect of synthesis parameters on the formation of these materials, the role of synthesis parameters in the evolution of TiO_2 and ZnO photocatalytic properties is still not entirely understood.

* e-mail: pattypgpatty@gmail.com

In this context, this study investigated the synthesis of titanium oxide and zinc oxide by different soft chemical methods and correlated the synthesis parameters with the material's photocatalytic activity, using RhB degradation as a probe reaction. Two different wet methods, sol-gel, and polymeric precursor methods[28,29], were studied regarding the photoactivity of the products. The aim of this study was to gain a better understanding of how the synthesis method affects the photocatalytic activity of TiO_2 and ZnO.

2. Experimental

2.1. Particle synthesis

ZnO and TiO_2 samples were prepared by the two different routes of ceramic processing: polymeric precursor (PP) and sol-gel (SG) methods. For the polymeric precursor method[29], in a typical procedure, citric acid ($HOC(CO_2H)(CH_2CO_2H)_2$, Alfa Aesar) was dissolved in 50 mL of distilled water preheated to 70 ºC under constant stirring. Then, titanium precursor or zinc precursor, titanium isopropoxide (Sigma-Aldrich) and zinc acetate (Ecibra), respectively, were added to this solution to promote the formation of a metal complex. The molar ratio of citric acid to metal (zinc or titanium) was set at 3:1. A proportion of 40:60 (wt%) of ethylene glycol ($HOCH_2CH_2OH$, Ecibra) to citric acid was then added to the solution to trigger a polymerization type reaction, which is desirable to improve the stability of the resulting complex. The solution was heated under constant stirring until a viscous resin was formed. This resulting solution was calcined at 300 ºC for 2 h to eliminate organic phase and volatile ions, followed by a crystallization treatment at 600 ºC, at a heating and cooling rate of 10 ºCmin^{-1}. For the precipitation route[28], samples were prepared by precipitating particles in a 0.025 molL^{-1} solution of each precursor separately, using ammonium hydroxide (NH_4OH P.A., Isofar) to pH control. Both solutions (zinc and titanium) were stabilized at pH equal 8. This reaction yielded in a white precipitate, which was isolated by centrifugation and washed with distilled water to remove residual reagents. Finally, the dry powder was calcined at 500 ºC for 2 h, using a heating and cooling rate of 5 ºCmin^{-1}.

2.2. Particles characterization

X-Ray diffraction was performed by the Shimadzu XRD 6000 equipment (Cu Kα) between 10 and 100°. The TiO_2 (JCPDS card n°. 21–1272) and ZnO (JCPDS card n°. 36–1451) lattice parameters were estimated by the Rietveld Refinement procedure[30]. The GSAS–EXPGUI software was utilized; and micrometric yttrium oxide (Sigma–Aldrich, 99.99%) was utilized as the pattern. In order to estimate the powders' crystallite size and lattice strain, The Williamson–Hall methodology was used[31]. The specific surface area (S.A.) by nitrogen physisorption, using the Brunauer, Emmett, and Teller (BET) method, was measured in a Micromeritics Gemini VII equipment. About 500 mg of the powder was previously prepared in Micromeritics Vap Prep 061, Sample Degas System. A degas was done at 100 ºC, with a heating at 10 ºC/min, with evacuation range in 5.0 mmHg/s at 60 min. The morphology was characterized by Field Emission Scanning Electron Microscopy (JEOL, JSM-6701F). KBr-pellets were examined by infrared spectroscopy technique in a Perkin-Elmer Spectrum 1000 spectrophotometer, with range to 4000 at 450 cm^{-1}.

2.3. Photocatalytic essays

RhB (Synth) was used as a probe dye for the photocatalytic essays. Suspensions containing 5.0 mgL^{-1} of RhB and 400 mgL^{-1} of ZnO or TiO_2 particles were prepared and irradiated during 90 min. The photocatalytic assays were performed in a batch reactor equipped with four Philips 15 W mercury lamps (UV-C, 254 nm). The reduction in dye concentration was estimated based on color removal, which was determined by spectrophotometry (Cary 60 UV-Vis, da Agilent spectrophotometer). Blank experiments carried out in RhB solution without particles (direct photolysis) showed the no occurrence of dye degradation in those conditions.

3. Results and discussion

3.1. Characterization

The X-Ray diffractograms are shown in Figure 1. No secondary phase was observed in the diffractograms. Thus, both synthesis methods evaluated in this work, PP and SG, were efficient to produce ZnO and TiO_2 with high levels of purity.

Moreover, regarding TiO_2 powders, only anatase phase was observed in the diffractograms. This result is desirable because it is the main TiO_2 polymorph applied to photocatalysis.

Figure 2 shows a comparison between the X–Ray experimental data and the profile adjusted by the Rietveld Refinement. These profiles were quite similar for all the samples, and the differences between them are close to a continuous line. Furthermore, all values for the convergence criterion χ^2 were close to the unity (ideality)[32]. Therefore, these results indicate that the quality of refinements was satisfactory for all the samples.

Table 1 shows the values of refined lattice parameters *a,b* (Å) and *c* (Å) compared to the theoretical ones from the crystallographic cards previously cited. In addition, the unit cell volumes *V* (Å^3) were also presented. It is noticed that the refined parameters are very similar when compared to the patterns. These results confirm the high crystallinity of the powders and great similarity with the indexed phases. The small differences observed for these values may be arising

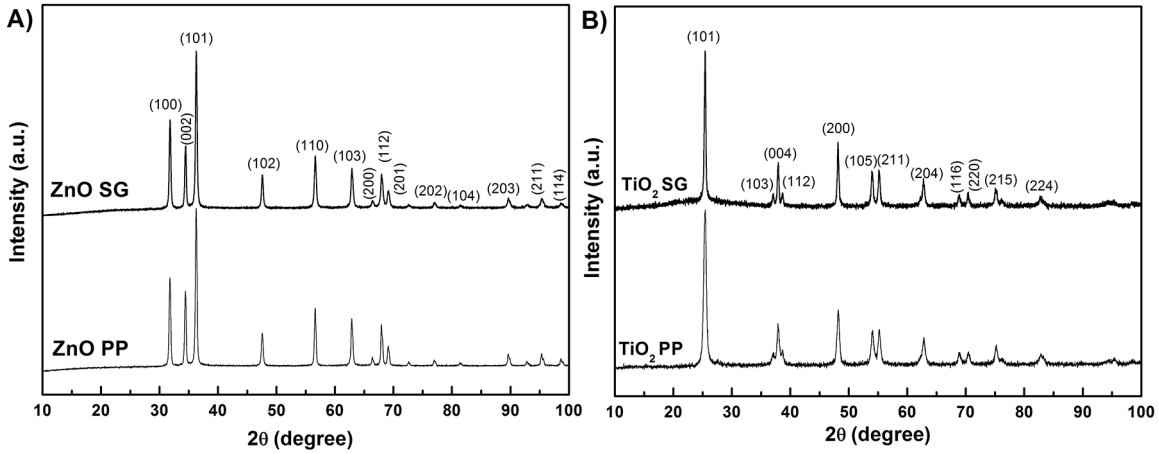

Figure 1. X–Ray diffractograms for A) ZnO powders and B) TiO_2 powders obtained by different methodologies.

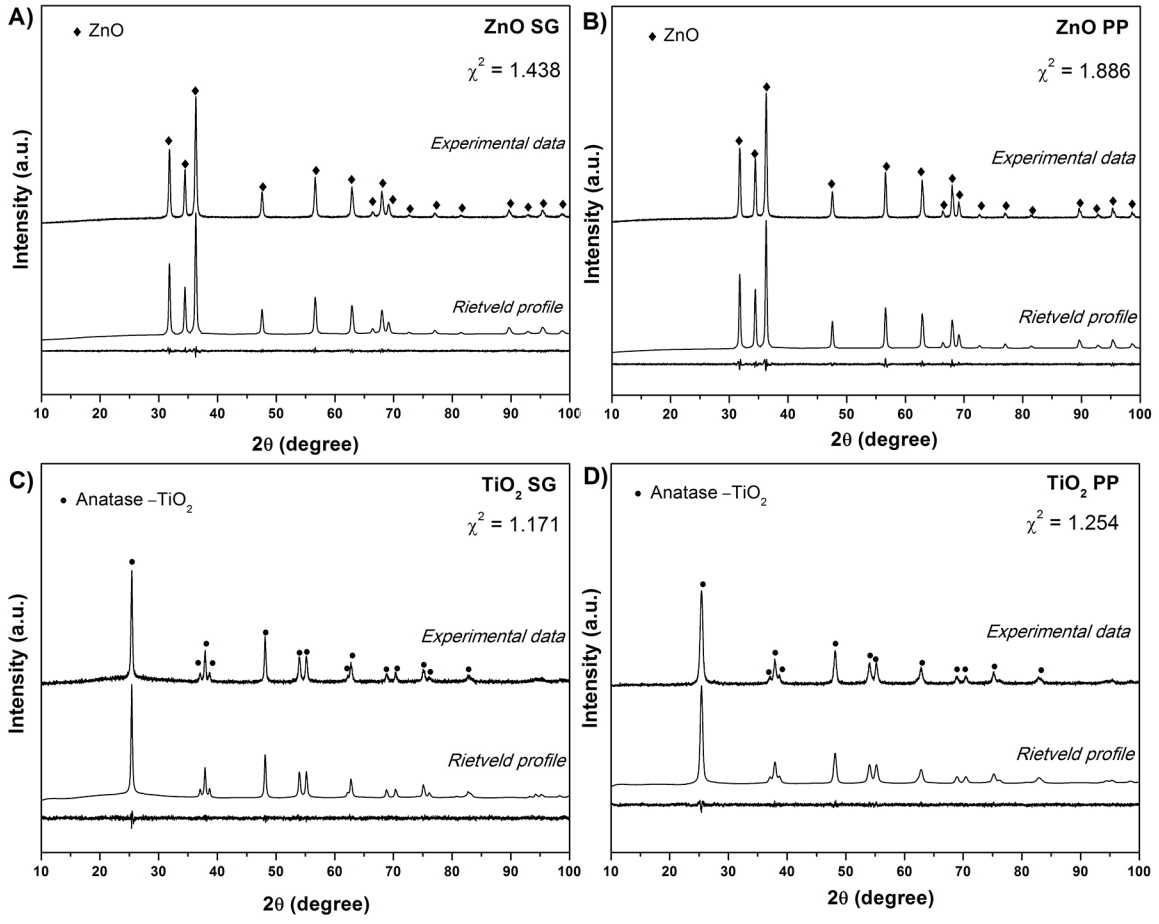

Figure 2. Comparison between the X-Ray experimental data and Rietveld profile for A) ZnO SG; B) ZnO PP; C) TiO_2 SG; and D) TiO_2 PP.

from ionic defects created during the synthesis, which can affect the values of lattice parameters and unit cell volume, consequently.

The values of average crystallite size *D (nm)* and lattice strain ε *(%)* estimated by means of Williamson-Hall methodology[31] are shown in Figure 3. All the samples showed nanometric crystallite sizes, which can be an indicative of small particles[33,34]. The samples obtained by the PP method have shown low values of lattice strain when compared to the ones obtained by the SG procedure. This phenomenon may

Table 1. Refined lattice parameters and unit cell volume for the ZnO and TiO_2 powders.

Sample	*a , b* (*A*)	*c* (*A*)	*V* (*Å³*)	*a , b* (*Å*)	*c* (*Å*)	*V* (*Å³*)
ZnO SG	3.2495	5.2056	47.603	**Pattern from JCPDS card (ZnO)**		
ZnO PP	3.2502	5.2072	47.639	3.2492	5.2054	47.593
TiO_2 SG	3.7877	9.5236	136.634	**Pattern from JCPDS card (TiO_2)**		
TiO_2 PP	3.7840	9.5111	136.190	3.7840	9.5140	136.228

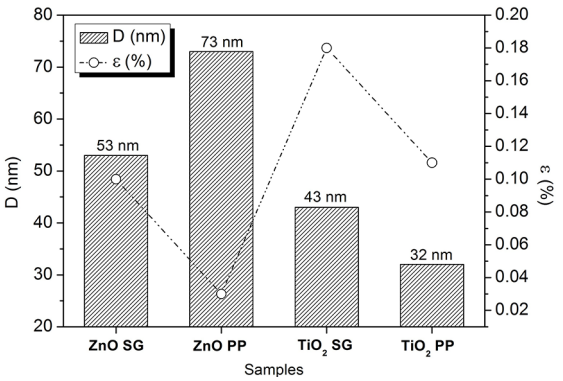

Figure 3. Values of crystallite size and lattice strain for the ZnO and TiO_2 powders.

be related to the creation of a smaller number of structural defects during the stage of synthesis, which tends to stress less the structure compared to the SG method.

Comparing the synthesis methods utilized to produce ZnO, the SG methodology has produced particles with smaller crystallite size (near 37%). Concerning samples composed by TiO_2, the powders obtained by polymeric precursors showed both lower crystallite sizes and lower lattice strain. Therefore, these results indicate that the TiO_2 particles produced by PP showed a lower quantity of structural defects, besides lower values of crystallite sizes.

Table 2 shows specific surface area data. ZnO SG and TiO_2 PP presented larger surface area.

The dimensions, morphology, and particle size distribution of ZnO and TiO_2 particles analyzed by FEG-SEM are presented in the images of Figure 4. Such images show nanometric particles for all samples and smaller particle size for ZnO SG and TiO_2 PP.

The ZnO SG particles (Figure 4A) were agglomerated but ordered and with a slightly faceted behavior, typical of the hexagonal structure of the wurtzite phase, found in X-ray diffraction (Figure 1A). This behavior was also observed

Table 2. Crystalline phase, surface area, and average particle size.

Sample	Crystalline phase	S.A. ($m^2.g^{-1}$)	Average particle size (nm)
ZnO SG	Wurtzite	5.55	47
ZnO PP	Wurtzite	4.35	86
TiO_2 SG	Anatase	9.57	49
TiO_2 PP	Anatase	10.91	20

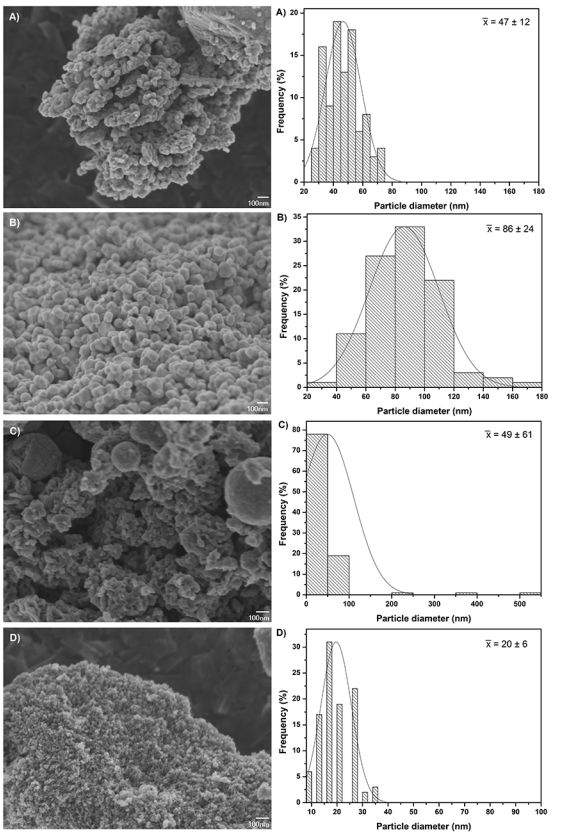

Figure 4. FEG-SEM microscopy and particle size diameter of A) ZnO SG, B) ZnO PP, C) TiO_2 SG, and D) TiO_2 PP.

in other studies, such as Nascimento et al.[35].Most of the particles had dimensions in the order of 40 nm, according to the histogram of particle size distribution represented by Figure 4A. In the study of Azam et al.[36], ZnO SG particles presented almost spherical shape and agglomeration, with diameters of about 20 nm. Arshad et al.[37], in turn, found pure ZnO SG particles, also of spherical morphology, but with larger sizes, with an average diameter of 55 nm, which are closer to those found in this work.

ZnO PP particles (Figure 4B) were structured in the same way as the ZnO SG particles, mostly with sizes of 80 nm approximately (Figure 4B). Guo et al.[38] found particles of pure ZnO PP, also of approximately spherical shape and diameters of 10 to 60 nm, relatively smaller but close to those found in the present work.

By analyzing comparatively the histograms present in Figure 4A and 4B, it can be identified that in the case of ZnO SG, the particle size distribution is more uniform and presents smaller size variation, from 25 to 75 nm, whereas the particle size of ZnO PP ranges from 20 to 180 nm. In addition, according to these histograms, the particle size of ZnO PP is larger, which corresponds to the fact that it has a smaller surface area (Table 2).

The TiO_2 SG particles had a size of about 45 nm (Figure 4C), irregular form and formation of spherical agglomerates (Figure 4C). TiO_2 PP particles, as shown in Figure 4D, were irregular, with apart agglomerations and smaller diameters than TiO_2 SG, with an average size of 20 nm (Figure 4D). From the images of Figure 4C and 4D, it is possible to observe that TiO_2 SG presented morphology with a higher porosity than TiO_2 PP.

According to the graphs presented in Figure 4C and 4D, the size variation of the TiO_2 SG particles is much larger than TiO_2 PP. TiO_2 SG presents two populations of the particle sizes: the main one with sizes from 20 to 100 nm (97%) and another around 500 nm. The latter correspond to agglomerates probably originated from nucleation and growth process of these particles during the synthesis and heat treatment. The particle sizes of TiO_2 PP appear much smaller, varying from 8 to 38 nm, which is consistent with its larger surface area.

Bahadur, Jain, and Pasricha[39] obtained values of average particle sizes for TiO_2 SG, in the range of 16 to 19 nm, different from this work. The average particle diameter of the TiO_2 PP found in Nascimento et al.[35] was 15 nm, a dimension quite compatible with those obtained in this work. Vargas et al.[40] detected TiO_2 PP particles of irregular shapes, with smooth edges and sizes of approximately 10 nm, also close to those of this study.

The average particle size of the synthesized oxides was directly related to their respective surface areas. According to the considerations made and the results presented, it is possible to observe this relation, in which the oxides that presented the higher surface area, TiO_2 PP and ZnO SG, presented smaller particle size.

Figure 5A shows the FTIR spectra of ZnO SG and ZnO PP. In these spectra, the intense bands observed are attributed to the stretching vibrations of the Zn-O bond appearing in the region of 445 and 465 cm^{-1}[41]. The wide bands located in the region of 3450 cm^{-1} and also the bands around 1625 cm^{-1} can be attributed to the vibrations of the O-H group. The bands at 2960 and 2930 cm^{-1} can be attributed to the symmetric stretching of the C-H groups. The other bands observed are relatively more intense in the spectra of the ZnO PP than in the ZnO SG. The O-C=O stretching is detected in 802 cm^{-1} and the bands around 1026, 1091, 1098, 1258, and 1379 cm^{-1} can be attributed to C-O or C-O-C vibration.

Figure 5B shows the spectra of TiO_2 SG and TiO_2 PP. The intense bands at 500 and 600 cm^{-1} correspond to the O-Ti-O bond[42]. The band observed at 1380 cm^{-1} corresponds to the C-H bond, which is relatively more intense in the TiO_2 PP sample.

According to the FTIR results, ZnO SG, ZnO PP, TiO_2 SG and TiO_2 PP showed, besides the functional groups characteristic of each oxide, other groups containing carbon and oxygen, except TiO_2 SG, which indicates the presence of organic residues of the precursors used in both synthetic methods. These residues persist even after heat treatment.

The presence of adsorbed species on the surface of the particles may influence their growth, since these species, due to steric hindrance, may prevent a greater contact between the particles and, consequently, they may have their growth prevented[43], resulting in a smaller particle size and larger surface area. This fact can be evidenced in the sample TiO_2 PP, which presented residual organic group in the FTIR spectrum (1380 cm^{-1}) at the same time that it exhibited smaller particle size and larger surface area than TiO_2 SG. In the case of the ZnO PP and ZnO SG samples, both presented organic residues in their spectra.

It is worth mentioning that a presence of organic residues that may influence particle growth, they can still compete with active sites on the surface of the nanoparticles, resulting in a lower catalytic activity.

For ZnO, the zinc acetate precursor proved to be a favorable precursor in obtaining the wurtzite phase, both in SG and PP. In the case of SG synthesis, the dissociation of the salt in the alcoholic medium allowed the complete formation of Zn^{2+}, and, with a controlled amount of water, the occurrence of hydrolysis and polycondensation with consequent formation of crystallites in the 53 nm range. In the case of PP method, the homogeneous distribution of the cations in the polymeric structure allowed, after heat treatment, crystallites formation with greater size than ZnO SG, 73 nm. However, the particles obtained by PP presented larger size than those obtained by SG. This result is justified by the higher heat treatment temperature in which the particles obtained by PP were submitted when compared to the SG method. This leads to the occurrence of the sintering process. In fact, the literature reports the phenomenon of sintering of nanoparticles of ZnO thermally treated at 500 ºC[41], which shows that the thermal treatment temperature promotes this phenomenon. In addition, the ZnO SG exhibited a larger surface area, which is consistent with its smaller particle size.

The titanium isopropoxide precursor was favorable in obtaining the anatase phase in both methods of synthesis for the TiO_2. However, it is believed that in the SG process it has uncontrolled hydrolysis, i.e. addition of excess water, which has probably provided abrupt precipitation, which may have turned the synthesis of difficult control of particle size. Consequently, the control of crystallite size and particle morphology becomes difficult. In fact, when comparing the size of crystallites and particles of TiO_2 obtained by SG and PP, the PP method promoted the formation of smaller

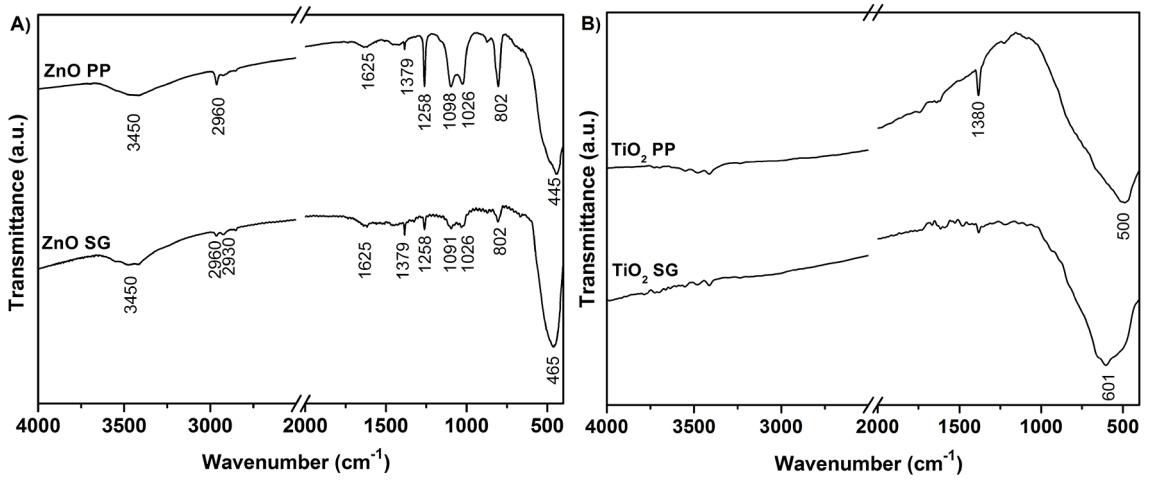

Figure 5. FTIR spectra of A) ZnO and B) TiO_2.

crystallites and particles than the same material obtained by SG. This is because the PP method promotes the complexation of the metal (in the case Ti^{4+}), which allowed greater control of the synthesis and consequently the formation of smaller crystallites. The formation of these smaller crystallites, in turn, allowed the formation of smaller particles, despite the higher heat treatment temperature in relation to the SG. In addition, TiO_2 PP presented higher surface area, which is consistent with the fact that it had a smaller average particle size, and organic residues on its surface (Figure 5B).

3.2. Photocatalysis

The synthesized nanoparticles were used in the photodegradation of RhB under UV-C irradiation. A similar experiment was also carried out in darkness in order to evaluate the RhB adsorption, however, no color removal was observed, indicating that adsorption could be neglected.

Figures 6 presents the photocatalytic tests results using the synthesized oxides, TiO_2 and ZnO, under UV-C irradiation.

ZnO and TiO_2 promoted color removal of the RhB solutions. These semiconductors are appropriate in photocatalytic reactions[15,44], promoting the kinetic represented in Figure 7.

According to Figure 6A, ZnO SG and ZnO PP promoted degradation of 88% of RhB within 180 minutes. Considering previously discussed data, ZnO SG had a much smaller particle size and a slightly larger surface area than ZnO PP (Table 2). However, these factors were not major in the photocatalytic properties, since, despite these discrete differences, both have the same photocatalytic efficiency. In addition, the results obtained by FTIR (Figure 5A) show that both samples have residues of synthesis adsorbed on their surface. These residues can compete with the active sites of the photocatalyst[43], and then impair the photocatalysis efficiency. Thus, although photocatalytic efficiency was significant, it could have been even better if the surface of the particles were free of residues of synthesis.

In the case of TiO_2 (Figure 6B), within 180 minutes, TiO_2 SG promoted degradation of 90% of RhB, while TiO_2 PP degraded 80%. Despite TiO_2 PP presenting smaller particle size and larger surface area than TiO_2 SG, this material had C-H species adsorbed on its surface (Figure 5B), possibly corresponding to residues of synthesis. This fact may have caused lower photocatalytic activity since these residues are competitors of active sites.

Once the discoloration of the dye was monitored in relation to the time, it was possible to calculate the reaction constant and the half-life time of the processes under study. Equation 1 relates the degradation time to the RhB concentration:

$$-\ln\left(\frac{RhB}{RhB_0}\right) = -\ln\left(\frac{C}{C_0}\right) = k't, \quad (1)$$

where $k' = k\,[SA]$, k is the velocity constant of the reaction, $[SA]$ is the concentration of active sites on the catalyst surface, t is the irradiation time, and RhB is equal to C, which represents the concentration of RhB dye[15].

The formation of radicals responsible for dye degradation is correlated to high velocity constant of the reaction (k') and low half-life time. However, for the constant k' to be high, which will influence the kinetics of degradation, the concentration of available active sites must also be high, since they are directly proportional, as can be seen in Equation 1.

Equation 2 allows the calculation of the time required to reduce by half of the concentration of organic compounds:

$$t_{1/2} = \frac{\ln 2}{k'}, \quad (2)$$

where $t_{1/2}$ is the half-life time[15].

According to Equation 1, $-ln(C/C_0)$ *versus* t represents a line with an angular coefficient equal to the velocity constant of the reaction, k'[15]. In Figures 7A and 7B, there is a graphical representation of $-ln(C/C_0)$ *versus* t where a first order kinetics can be identified for all cases, indicating that all the degradations have the same mechanism.

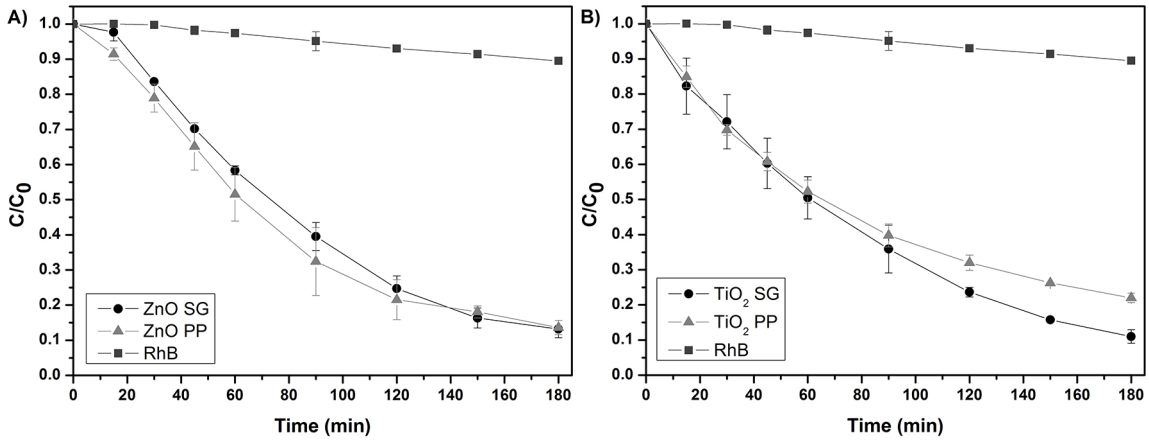

Figure 6. Evolution of the relative concentration of RhB as a function of the irradiation time relative to A) ZnO and B) TiO_2.

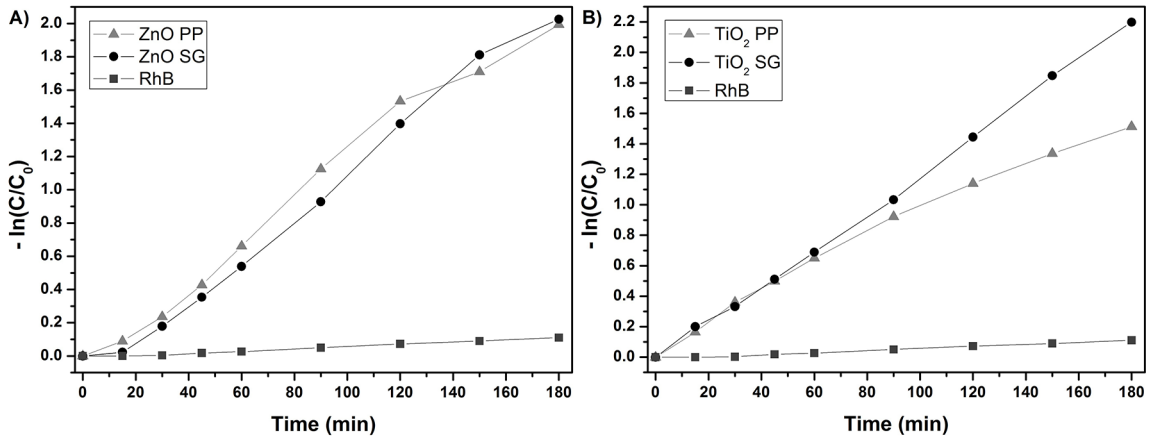

Figure 7. First order kinetics referent to the Rhodamine B degradation in different catalysts: A) ZnO and B) TiO_2.

Table 3 contains the values of *k'* obtained from Figures 7A and 7B, and their respective half-life times, calculated by Equations 1 and 2, respectively. For ZnO, the reactions presented values of *k'* and $t_{1/2}$ quite close. On the other hand, the values of *k'* and $t_{1/2}$ of TiO_2 have been shown to be relatively distinct, with TiO_2 SG being highlighted with the highest *k'* and consequently smaller $t_{1/2}$, and therefore with the higher velocity of photodegradation. This is because TiO_2 PP presents organic residues adsorbed on its surface, as evidenced previously, thus causing less photocatalytic activity even with smaller particle size and greater surface area. In addition, it is worth mentioning that TiO_2 SG presented identical values of *k'* and $t_{1/2}$ to those of ZnO PP. Both oxides are therefore equally efficient in the degradation of the dye under study.

Table 3. Values of *k'*, R^2, and $t_{1/2}$ of the samples under UV-C irradiation.

Sample	*UV-C irradiation*		
	k' (min^{-1})	R^2	$t_{1/2}$ *(min)*
ZnO SG	$1.19.10^{-2}$	0.985	58
ZnO PP	$1.23.10^{-2}$	0.988	56
TiO_2 SG	$1.23.10^{-2}$	0.998	56
TiO_2 PP	$8.4.10^{-3}$	0.984	82

4. Conclusions

The methods of synthesis of PP and SG allowed obtaining ZnO and TiO_2. Both methodologies resulted in the same crystalline phases for TiO_2 and ZnO, despite different thermal treatments. TiO_2 PP and ZnO SG had a higher surface area and a smaller average particle size. Furthermore, in both methods, organic residues were identified, indicating that higher heat treatment temperatures would be adequate to eliminate these residues since they influence the photocatalysis by competing with active sites on the surface of the materials.

TiO_2 SG was outstanding in the photocatalytic tests due to the greater degradation of the RhB dye. TiO_2 PP, even having a larger surface area and smaller particle size, provided lower degradation and photocatalytic activity due to the presence of organic residues on its surfaces.

5. Acknowledgments

The authors gratefully acknowledge the Brazilian research funding programs and agencies CNPq (proc. 444117/2014-8), CAPES, and FAPEMIG for their financial backing. We are also grateful to the Federal University of Alfenas and Embrapa Instrumentação Agropecuária, São Carlos.

6. References

1. Lončarević D, Dostanić J, Radonjić V, Živković L, Jovanović DM. Simultaneous photodegradation of two textile dyes using TiO_2 as a catalyst. *Reaction Kinetics, Mechanisms and Catalysis*. 2016;118(1):153-164. DOI: 10.1007/s11144-016-0990-0

2. Li Y, Zhang WP, Li X, Yu Y. TiO_2 nanoparticles with high ability for selective adsorption and photodegradation of textile dyes under visible light by feasible preparation. *Journal of Physics and Chemistry of Solids*. 2014;75(1):86-93. DOI: 10.1016/j.jpcs.2013.08.012

3. Kaur J, Kumar V, Gupta K, Bansal S, Singhal S. A facile strategy for the degradation of recalcitrant textile dyes using highly robust ZnO catalyst. *Journal of Chemical Technology and Biotechnology*. 2016;91(8):2263-2275. DOI: 10.1002/jctb.4812

4. Bhatia S, Verma N, Bedi RK. Optical application of Er-doped ZnO nanoparticles for photodegradation of direct red - 31 dye. *Optical Materials*. 2016;62:392-398. DOI: 10.1016/j.optmat.2016.10.013

5. Brites FF, Santana VS, Fernandes-Machado NRC. Effect of Support on the Photocatalytic Degradation of Textile Effluents Using Nb_2O_5 and ZnO: Photocatalytic Degradation of Textile Dye. *Topics in Catalysis*. 2011;54(1):264-269. DOI: 10.1007/s11244-011-9657-2

6. Prado AGS, Bolzon LB, Pedroso CP, Moura AO, Costa LL. Nb_2O_5 as efficient and recyclable photocatalyst for indigo carmine degradation. *Applied Catalysis B: Environmental*. 2008;82(3-4):219-224. DOI: 10.1016/j.apcatb.2008.01.024

7. Xu H, Zhang Y, Jiang Q, Reddy N, Yang Y. Biodegradable hollow zein nanoparticles for removal of reactive dyes from wastewater. *Journal of Environmental Management*. 2013;125:33-40. DOI: 10.1016/j.jenvman.2013.03.050

8. Carneiro PA, Osugi ME, Sene JJ, Anderson MA, Zanoni MVB. Evaluation of color removal and degradation of a reactive textile azo dye on nanoporous TiO_2 thin-film electrodes. *Electrochimica Acta*. 2004;49(22-23):3807-3820. DOI: 10.1016/j.electacta.2003.12.057

9. Gupta VK, Ali I, Saleh TA, Nayak A, Agarwal S. Chemical Treatment Technologies for Waste-Water Recycling - An Overview. *ChemInform*. 2012;43(45):6380-6388. DOI: 10.1002/chin.201245270

10. Alzahrani E. Zinc Oxide Nanopowders Prepared by the Sol-Gel Process for the Efficient Photodegradation of Methyl Orange. *Current Analytical Chemistry*. 2016;12(5):465-475. DOI: 10.2174/1573412912666160104234348

11. Tolosana-Moranchel A, Casas JA, Carbajo J, Faraldos M, Bahamonde A. Influence of TiO_2 optical parameters in a slurry photocatalytic reactor: Kinetic modelling. *Applied Catalysis B: Environmental*. 2016;200:164-173. DOI: 10.1016/j.apcatb.2016.06.063

12. Paszkiewicz M, Luczak J, Lisowski W, Patyk P, Zaleska-Medynska A. The ILs-assisted solvothermal synthesis of TiO_2 spheres: The effect of ionic liquids on morphology and photoactivity of TiO_2. *Applied Catalysis B: Environmental*. 2016;184:223-237. DOI: 10.1016/j.apcatb.2015.11.019

13. Savastenko NA, Filatov II, Lyushkevich VA, Chubrik NI, Gabdullin MT, Ramazanov TS, et al. Enhancement of ZnO-Based Photocatalyst Activity by RF Discharge-Plasma Treatment*. *Journal of Applied Spectroscopy*. 2016;83(5):757-763. DOI: 10.1007/s10812-016-0359-1

14. Kaur J, Bhukal S, Gupta K, Tripathy M, Bansal S, Singhal S. Nanocomposite of CeO_2 and ZnO: An active material for the treatment of contaminated water. *Materials Chemistry and Physics*. 2016;177:512-520. DOI: 10.1016/j.matchemphys.2016.04.063

15. Rahman QI, Ahmad M, Misra SK, Lohani M. Effective photocatalytic degradation of rhodamine B dye by ZnO nanoparticles. *Materials Letters*. 2013;91:170-174. DOI: 10.1016/j.matlet.2012.09.044

16. Carneiro JO, Samantilleke AP, Parpot P, Fernandes F, Pastor M, Correia A, et al. Visible Light Induced Enhanced Photocatalytic Degradation of Industrial Effluents (Rhodamine B) in Aqueous Media Using TiO_2 Nanoparticles. *Journal of Nanomaterials*. 2016;2016:4396175. DOI: 10.1155/2016/4396175

17. Torbrügge S, Ostendorf F, Reichling M. Stabilization of Zinc-Terminated ZnO(0001) by a Modified Surface Stoichiometry. *Journal of Physical Chemistry C*. 2009;113(12):4909-4914. DOI: 10.1021/jp804026v

18. Wang L, Chang L, Zhao B, Yuan Z, Shao G, Zheng W. Systematic Investigation on Morphologies, Forming Mechanism, Photocatalytic and Photoluminescent Properties of ZnO Nanostructures Constructed in Ionic Liquids. *Inorganic Chemistry*. 2008;47(5):1443-1452. DOI: 10.1021/ic701094a

19. Perez-Lopez OW, Farias AC, Marcilio NR, Bueno JMC. The catalytic behavior of zinc oxide prepared from various precursors and by different methods. *Materials Research Bulletin*. 2005;40(12):2089-2099. DOI: 10.1016/j.materresbull.2005.07.001

20. Cao LX, Spiess FJ, Huang AM, Suib SL, Obee TN, Hay SO, et al. Heterogeneous Photocatalytic Oxidation of 1-Butene on SnO_2 and TiO_2 Films. *The Journal of Physical Chemistry B*. 1999;103(15):2912-2917. DOI: 10.1021/jp983860z

21. Amorim C, Keane MA. Effect of surface acid groups associated with amorphous and structured carbon on the catalytic hydrodechlorination of chlorobenzenes. *Journal of Chemical Technology & Biotechnology*. 2008;83(5):662-672. DOI: 10.1002/jctb.1846

22. Xiong G, Wang X, Lu L, Yang X, Xu Y. Preparation and Characterization of Al_2O_3–TiO_2 Composite Oxide Nanocrystals. *Journal of Solid State Chemistry*. 1998;141(1):70-77. DOI: 10.1006/jssc.1998.7917

23. McLaren A, Valdes-Solis T, Li G, Tsang SC. Shape and Size Effects of ZnO Nanocrystals on Photocatalytic Activity. *Journal of the American Chemical Society*. 2009;131(35):12540-12541. DOI: 10.1021/ja9052703

24. Han S, Choi S, Kim SS, Cho M, Jang B, Kim DY, et al. Low-Temperature Synthesis of Highly Crystalline TiO_2 Nanocrystals and their Application to Photocatalysis. *Small*. 2005;1(8-9):812-816. DOI: 10.1002/smll.200400142

25. Xie RC, Shang JK. Morphological control in solvothermal synthesis of titanium oxide. *Journal of Materials Science*. 2007;42(16):6583-6589. DOI: 10.1007/s10853-007-1506-0

26. Yu J, Yu X. Hydrothermal Synthesis and Photocatalytic Activity of Zinc Oxide Hollow Spheres. *Environmental Science & Technology*. 2008;42(13):4902-4907. DOI: 10.1021/es800036n

27. Zeng JH, Jin BB, Wang YF. Facet enhanced photocatalytic effect with uniform single-crystalline zinc oxide nanodisks. *Chemical Physics Letters*. 2009;472(1-3):90-95. DOI: 10.1016/j.cplett.2009.02.082

28. Bahnemann DW, Kormann C, Hoffmann MR. Preparation and characterization of quantum size zinc oxide: a detailed spectroscopic study. *The Journal of Physical Chemistry*. 1987;91(14):3789-3798. DOI: 10.1021/j100298a015

29. Rodríguez-Paéz JE, Caballero AC, Villegas M, Moure C, Durán P, Fernández JF. Controlled precipitation methods: formation mechanism of ZnO nanoparticles. *Journal of the European Ceramic Society*. 2001;21(7):925-930. DOI: 10.1016/S0955-2219(00)00283-1

30. Rietveld HM. Line profiles of neutron powder-diffraction peaks for structure refinement. *Acta Crystallographica*. 1967;22:151-152. DOI: 10.1107/S0365110X67000234

31. Williamson GK, Hall WH. X-ray line broadening from filed aluminum and wolfram. *Acta Metallurgica*. 1953;1(1):22-31. DOI: 10.1016/0001-6160(53)90006-6

32. Toby BH. R factors in Rietveld analysis: How good is good enough? *Powder Diffraction*. 2006;21(01):67-70. DOI: 10.1154/1.2179804

33. Lu K, Manjooran N, Radovic M, Pickrell G, Medvedovski E, Olevski E, et al. *Advances in nanomaterials and nanostructures*. Hoboken: Wiley; 2011. 206 p.

34. Akbari B, Tavandashti MP, Zandrahimi M. Particle size characterization of nanoparticles – a practical approach. *Iranian Journal of Materials Science & Engineering*. 2011;8(2):48-56.

35. Nascimento GS, Mambrini GP, Paris EC, Peres JA, Colnago LA, Ribeiro C. Evaluation of the catalytic activity of oxide nanoparticles synthesized by the polymeric precursor method on biodiesel production. *Journal of Materials Research*. 2012;27(23):3020-3026. DOI: 10.1557/jmr.2012.349

36. Azam A, Ahmed F, Arshi N, Chaman M, Naqvi AH. Formation and characterization of ZnO nanopowder synthesized by sol–gel method. *Journal of Alloys and Compounds*. 2010;496(1-2):399-402. DOI: 10.1016/j.jallcom.2010.02.028

37. Arshad M, Azam A, Ahmed AS, Mollah S, Naqvi AH. Effect of Co substitution on the structural and optical properties of ZnO nanoparticles synthesized by sol–gel route. *Journal of Alloys and Compounds*. 2011;509(33):8378-8381. DOI: 10.1016/j.jallcom.2011.05.047

38. Guo BL, Han P, Guo LC, Cao YQ, Li AD, Kong JZ, et al. The Antibacterial Activity of Ta-doped ZnO Nanoparticles. *Nanoscale Research Letters*. 2015;10:336. DOI: 10.1186/s11671-015-1047-4

39. Bahadur N, Jain K, Pasricha R, Govind, Chand S. Selective gas sensing response from different loading of Ag in sol–gel mesoporous titania powders. *Sensors and Actuators B: Chemical*. 2011;159(1):112-120. DOI: 10.1016/j.snb.2011.06.058

40. Vargas MA, Franco Y, Ochoa Y, Ortegón Y, Rodriguez Paez JE. TiO_2 sintetizado por el método de precursor polimerico (Pechini): estructura de la resina intermedia. *Boletín de la Sociedad Española de Cerámica y Vidrio*. 2011;50(5):267-272. DOI: 10.3989/cyv.352011

41. Giraldi TR, Santos GV, Mendonça VR, Ribeiro C, Weber IT. Annealing Effects on the Photocatalytic Activity of ZnO Nanoparticles. *Journal of Nanoscience and Nanotechnology*. 2011;11(4):3635-3640. DOI: 10.1166/jnn.2011.3801

42. Costa ACFM, Vilar MA, Lira HL, Kiminami RHGA, Gama L. Síntese e caracterização de nanopartículas de TiO_2. *Cerâmica*. 2006;52(324):255-259. DOI: 10.1590/s0366-69132006000400007

43. Giraldi TR, Santos GVF, de Mendonca VR, Ribeiro C, Weber IT. Effect of synthesis parameters on the structural characteristics and photocatalytic activity of ZnO. *Materials Chemistry and Physics*. 2012;136(2-3):505-511. DOI: 10.1016/j.matchemphys.2012.07.018

44. Wang L, Li J, Wang Y, Zhao L, Jiang Q. Adsorption capability for Congo red on nanocrystalline MFe_2O_4 (M=Mn, Fe, Co, Ni) spinel ferrites. *Chemical Engineering Journal*. 2012;181-182:72-79. DOI: 10.1016/j.cej.2011.10.088